2017-12

Offshore monopile in the southern North Sea: Part I, calibrated input sea state

Edesess, Ariel

10.1680/jmaen.2017.14
Proceedings of the Institution of Civil Engineers - Maritime Engineering
Thomas Telford Ltd.

Maritime Engineering

Offshore monopile in the southern North Sea: Part I, calibrated input sea state

ice | proceedings

Proceedings of the Institution of Civil Engineers
Pages 1–14

Keywords: offshore wind farm maintenance / free surface flow / significant wave height / spectral analysis / ocean wave statistics / renewable energy / crew transfer vessel / OpenFOAM® / waveFoam

Offshore monopile in the southern North Sea: Part I, calibrated input sea state

Ariel J. Edesess MSc
Department of Civil and Environmental Engineering,
University College Cork,
College Road,
Cork, Ireland
Denis Kelliher PhD
Department of Civil and Environmental Engineering,
College Road,
University College Cork,
Cork, Ireland

Alistair G. L. Borthwick PhD, DSc, Dr *h.c.*, FICE, FREng, FRSE
School of Engineering,
The University of Edinburgh,
The King's Buildings
Edinburgh, EH9 3JL, U.K.
Gareth P. Thomas PhD
Department of Applied Mathematics,
Western Gateway Building,
Western Road,
University College Cork,
Cork, Ireland

Safe, reliable access is an essential precondition for the successful maintenance of offshore wind farms. Access from vessels to wind turbines depends upon the severity of the sea state in the vicinity of the turbine support structure. This paper presents a validation of a numerical boundary condition developed to reproduce the seasonal sea state at Teesside Offshore Wind Farm, off the coast of the United Kingdom. The boundary condition, called *customSpectrum*, is derived from wave energy spectra obtained by analysis of existing field measurements of wave free surface displacement at the wind farm site and implemented in OpenFOAM®, the open-source computational fluid dynamics (CFD) library. OpenFOAM® is then used to simulate typical spring, summer, autumn and winter sea states as uni-directional waves. Predicted surface elevations and significant wave heights are found to be in agreement with *in situ* buoy data, thus validating the OpenFOAM® model. Satisfactory agreement is achieved between analytical and numerically predicted spectral density functions for the horizontal and vertical water particle velocity components. It is found that the wave activity at Teesside is uni-modal in spring and autumn, and bi-modal in summer and winter. It is recommended to extend the procedure to multi-directional waves in crossing seas.

1. Introduction

Global efforts to reduce CO_2 emissions are likely to cause a decline in energy production by large coal and gas power plants, accompanied by increasing development of clean energy production methods. By June 2015, 164 countries had adopted some form of renewable energy target to decrease carbon emissions (Kieffer & Couture, 2015). Of the marine renewable energy sources available, offshore wind power is one of the most economic and fastest growing. Whilst estimates vary, it appears that offshore wind is a global resource with great potential: Krewitt *et al.* (2009) assessed the technical potential of offshore wind energy to be approximately 16,000 (TW.h).a^{-1} by 2050 and Capps & Zender (2010) more recently calculated the overall global value of offshore wind energy to be approximately 340,000 (Tw.h)a^{-1}. At the beginning of 2016, the European grid had more than 3,000 offshore wind turbine connections (Pineda, 2016). The potential for offshore wind is particularly favourable in areas such as Northern Europe, where excellent offshore conditions with steady high winds and a suitable sea floor can be found in many locations.

A significant hindrance to the growth of offshore wind farms arises from difficulties faced in maintaining the turbines, which may be located on monopiles 30-50 km from the shore (or onshore base) and in water up to 30 m deep (Corbetta *et al.*, 2014; Sperstad *et al.*, 2014). Maintenance difficulties can occur even for near-shore wind farms; it was estimated recently that, for a wind farm off the coast of Ireland, the turbines were only accessible for repairs for 50-75% of the year (Breton & Moe, 2009; van Bussel *et al.*, 2001). Additional costs are incurred from hiring repair workers and vessels to transport the workers to the turbines. Overall, operations and maintenance (O&M) costs can account for 25-50% of total energy production costs (Dalgic *et al.*, 2015a; Maples *et al.*, 2013). The rapid development of offshore wind farms has outpaced research and there is a lack of consensus on the best methods for access and maintenance (van Bussel *et al.*, 2001; Baagøe-Engels & Stentoft, 2016; Browell *et al.*, 2016). As a consequence, there is an increased risk of hazard to workers and substantial economic loss due to uncompleted repairs.

Several methods are employed by maintenance personnel to access offshore wind turbines, the method selected depending on cost and type of repair required. Access methods include helicopter, service operations vessel and crew transfer vessel (CTV). Helicopters have the advantage that they are not affected by wave conditions, but have the following significant drawbacks: bulky equipment cannot be transported, the number of personnel is limited due to space and the hire cost, which is at least five times greater than a CTV (Auckland & Garlick, 2015). Service operations vessels are useful for carrying heavy equipment and transporting a larger number of repair workers but again have the disadvantage over other access methods of increased cost. A common and economic method to transfer workers is by smaller CTVs, which account for 46% of the methods used (Dalgic *et al.*, 2015a). CTVs include monohulls, catamarans and small-waterplane-area twin hull (SWATH) type vessels. The different types of CTV offer various benefits including lower cost, capability of transferring large equipment such as cranes and sufficient space for a large fleet of maintenance personnel (Auckland & Garlick, 2015). Typically, the limiting sea state factor for crew transfer vessels is that $H_s \leq 1.5$ m, where H_s is the significant wave height (Halvorsen-Weare *et al.*, 2013; Dalgic *et al.*, 2015b). In general, the use of the significant wave height parameter as the main access criterion introduces additional uncertainty because H_s depends on *in situ* wind and wave conditions and also on the wave field in the near-wake of the turbine monopile (Sperstad *et al.*, 2014). Using H_s as the sole discerning factor provides no information on the modality of the sea state, which is subject to seasonal changes. These additional variables imply that the significant wave height may not provide sufficient information from which to determine the safety of the crew members and the stability of the crew transfer vessel under operational conditions (Edesess *et al.*, 2017b). Moreover, methods of determining H_s vary between wind farms and, to the authors' knowledge, no regulation exists by which to determine H_s; a survey conducted by Hoffman (2011) found a total of 49 different models for maintenance strategies were used by offshore wind energy companies.

In order to access the turbines, the CTV is driven towards the turbine monopile and, under steady thrust from the engine, contact between the turbine transition piece and the CTV is maintained by frictional forces. Representative monopiles have a single turbine transition piece, ideally located downstream of the principle wave direction, where the vessel is driven upwind. Changes in the near-wake flow field where the CTV lies can result in a weakening of the frictional force and CTV "slippage", where the vessel becomes dislodged from the turbine, potentially endangering crew members in transition or resulting in incomplete maintenance and large economic losses. Prediction of CTV motions under operating conditions requires knowledge of the hydrodynamics and water particle kinematics within the near-wake.

To the present authors' knowledge, no experimental data exist describing typical vessel motions during crew transfer, and there is only limited research concerning the hydrodynamic forces on a floating body located within the wake of a fixed body, where frictional forces instead of mooring lines are used to maintain contact. Josse *et al.* (2011) presented a system in which hydrodynamic forces were ignored and the angle of the vessel against the monopile turbine was assumed to be the only parameter affecting the frictional contact. Although this approach was not validated, Josse *et al.* (2011) determined that wave frequency was a critical factor affecting motion and commented on the need for an improved hydrodynamic analysis of the effect of incident wave frequencies on vessel loading. König *et al.* (2017) also emphasised the necessity of calculating the hydrodynamic forces incident on the vessel and presented the results for two wave frequencies. As expected, they found that the influence of the monopile on the

flow field decreases as the wave period increases. However, they did not determine a limiting wave period beyond which the CTV could no longer operate. Moreover, their work focused primarily on the influence of the monopile in monochromatic wave fields in an experimental setting.

The hydrodynamic forces, which are a function of the incident wave period, the wave height and monopile diameter, aid in identifying the limiting conditions under which the vessel remains in contact with the monopile turbine. The limiting condition is when the total vertical hydrodynamic forces on the vessel overcome the frictional contact force between the vessel fender and the transition piece on the monopile turbine (König *et al.*, 2017; Edesess *et al.*, 2017a). An improvement to the previous work in this area would determine the hydrodynamic force in an irregular sea state representing the conditions at an operational offshore wind farm.

To determine CTV response in the future, it is first necessary to numerically simulate the correct sea state. The focus herein is therefore on simulating an accurate representation of a specific undisturbed sea state, rather than relying on a parametric representation of the sea state. Parametric representations of the sea state do not provide information on the bi-modality or uni-modality of a wave field, which can be altered throughout the different seasons in a year and are location-dependent. This is the first of two papers dealing with the subject of accurate representation of the local wave field an offshore wind farm.

The open-source C++ library of fluid dynamics solvers, OpenFOAM®, has been developed by the CFD community to simulate many types of flow, including multi-phase flows. The present paper describes an input boundary condition for simulating uni-directional free surface wave motions in the open sea for seasonal sea states utilising wave buoy displacement data acquired *in situ* from Teesside Offshore Wind Farm (see Figure 1 for location and array set-up), and which were made available by the operations team at EDF Energy Renewables. Comparisons between the simulated sea state and observed wave data, provided directly from the practitioners, is used to validate the boundary condition and numerically determine the numerical sea state and wave particle kinematics at the wind farm.

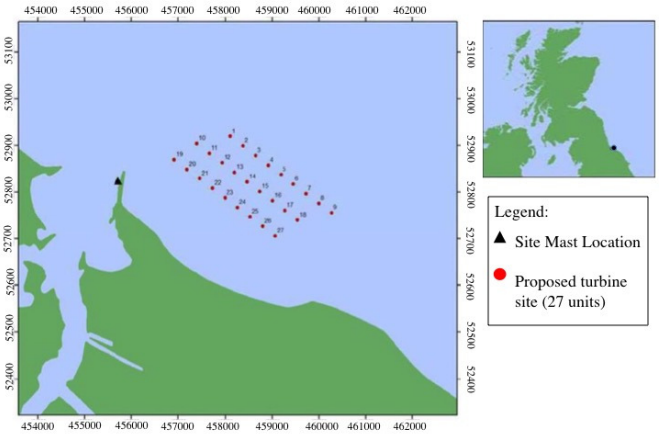

Figure 1. Location of Teesside Offshore Wind Farm; Image provided by EDF Energy Renewables

2. Governing Equations

It is assumed that the uni-directional sea state can be represented as a linear superposition of regular waves, each being of small slope and possessing a random phase. The validity of the linear wave assumption is confirmed by the Le Méhauté diagram (Le Mehaute, 1976). The incident waves are described in the frequency domain by a spectrum of the discrete wave amplitudes, derived by applying a Fast Fourier Transform (FFT) to the observed free surface displacement time series. From the FFT, the continuous energy, or wave, spectrum is calculated. The total energy (m_0) within the wave spectrum is defined as the area underneath the spectral curve and is equivalent to the variance of the surface elevation (Papoulis, 1991; Sumer & Fredsøe, 2006),

$$(1) \qquad m_0 = \int_0^\infty S_\eta(f)df = \sigma_\eta^2,$$

where σ_η^2 is the variance of the displacement data and S_η is the spectral value ($^{m^2}/_{Hz}$), and f is the frequency in Hz. The significant wave height and the amplitude components of the frequency spectrum can be found from

$$(2) \qquad H_s = 4\sqrt{m_0}$$

and

$$(3) \qquad a_n = \sqrt{2S(f_n)df},$$

where the subscript n refers to the value at the n-th frequency component. The free surface elevation and particle kinematics of a two-dimensional irregular sea state in the (x,z)-plane are then described analytically from linear wave theory (Dean & Dalrymple, 1991) by

$$\eta = \sum_n a_n \cos\left(k_n x - \omega_n t + \psi_n\right) \tag{4}$$

$$u = \sum_n a_n \omega_n \frac{\cosh k_n\left(z+h\right)}{\sinh k_n h} \cos\left(k_n x - \omega_n t + \psi_n\right) \tag{5}$$

$$w = \sum_n a_n \omega_n \frac{\sinh k_n\left(z+h\right)}{\sinh k_n h} \sin\left(k_n x - \omega_n t + \psi_n\right), \tag{6}$$

where η is the irregular surface elevation, u and w are the water particle velocity components in the horizontal and vertical directions, ω_n is the n-th wave angular frequency component, z is the location measured vertically upwards from mean water level, h is the mean water depth, x is the distance in the incident wave direction and the wave number k_n is related to ω_n through the linear dispersion relation, $\omega_n^2 = g k_n \tanh(k_n h)$, where g is acceleration due to gravity. The quantity ψ_n, for each n, is a random phase lying in the range $0 \leq \psi_n < 2\pi$. The velocity components can be used for calculations of the vessel body motion, for which the horizontal and vertical accelerations and wave pressure are also useful parameters.

Equation (1) is used to check that the calculated sea state given by (4) correctly corresponds to the original wave spectrum, when converting from the frequency domain to the time domain, and hence that the spectrum provides a correct representation of the original displacement time series. A moving-average filter with a minimum of 8 input points is used to smooth the spectrum.

3. Numerical Method

The sea state is simulated numerically in OpenFOAM® using a modification of the multiphase finite volume solver, *interFoam*, contained within the Waves2Foam package release (Jacobsen *et al.*, 2011). At the inlet, a Dirichlet boundary condition is applied using a prescribed free surface elevation and water particle velocity component values at cells on the boundary face, determined using Stokes 1st-order wave theory from equations (4)-(6). A slip boundary condition is applied at the bottom of the domain. The solver included in the Waves2Foam package, *waveFoam*, couples the Reynolds-averaged continuity and Navier-Stokes momentum equation to the volume of fluid (VOF) method to calculate the motions of both air and water (Jacobsen *et al.*, 2011). The governing equations for multiphase incompressible flow are listed below as follows: the continuity equation is

$$\nabla \cdot \mathbf{u} = 0 \tag{7}$$

and the momentum equation is

$$\rho \frac{\partial \mathbf{u}}{\partial t} + \rho \nabla \cdot \left[\mathbf{u}\mathbf{u}^T\right] = -\nabla p^* - \rho \mathbf{g} + \rho \nabla \cdot \left[\mu \nabla \mathbf{u} + \tau\right] + \gamma_T \kappa_\alpha \nabla \alpha. \tag{8}$$

In the absence of surface tension, γ_T, $\mathbf{u} = (u, v, w)$ is the velocity field, p^* is the pressure in excess of hydrostatic, τ is the Reynolds stress tensor, $\mathbf{g}$ acts in the vertical direction only. The quantity α is the volume of fluid fraction scalar field used for the multiphase flow, which has a fixed value dependent on the ratio of water-to-air in the boundary cell where

$$\alpha = \begin{cases} 0, & \text{air} \\ 1, & \text{water} \\ 0 \leq \alpha \leq 1, & \text{interface} . \end{cases}$$

Equations (7) and (8) and the Dirichlet wave velocity boundary condition are discretized in space using the finite volume method and time-integrated to give the sea state as a free surface displacement and water particle velocity time series.

3.1. Wave absorption

Wave reflection from a solid wall boundary is eliminated by means of a relaxation zone, which acts as a sponge layer to absorb incoming waves. Within the relaxation zone, a relaxation function α_R, given by

$$\alpha_R\left(\chi_R\right) = 1 - \frac{\exp\left(\chi_R^\mu\right) - 1}{\exp(1) - 1} \quad \text{for} \quad \chi_R \in [0; 1] \tag{9}$$

is calculated where χ_R is 0 at the start of the relaxation zone and 1 at the end. Inside the relaxation zone, the wave is absorbed through the function

$$q = \alpha_R q_{computed} + (1 - \alpha_R) q_{target}, \quad (10)$$

in which q is either the fluid volume fraction or the velocity $\mathbf{u}$, where $\mathbf{u}_{target} = \mathbf{0}$. The value of μ can be adjusted to alter the behaviour of the outgoing wave and shorten the relaxation zone. A value of $\mu = 1$ allows more rapid wave absorption and a shorter relaxation zone with a length of less than one wavelength, without disrupting the inlet waves (Edesess *et al.*, 2017a). The relaxation zone is positioned at the outlet of the computational domain to absorb outgoing waves.

3.2. Case set-up

The horizontal dimensions of the computational domain were set according to the maximum wavelength desired as approximately $4\lambda_p$ in the wave direction and λ_p in the transverse direction, where λ_p is the wavelength corresponding to the modal wave period, T_p. When two values of T_p are evident (as for the bi-modal spectrum produced in the winter dataset), the larger wave period value is taken as the modal period for the purpose of ensuring the computational domain and simulation duration are of sufficient length. A relaxation zone of length λ_p was located at the outlet. The vertical dimension comprised 15 m still water depth, with a further 10 m of air above the water free surface to avoid surface diffusion. A cut-off frequency was employed to remove the longest wavelengths in the low energy part of the spectrum and hence keep the computational domain from having to be too long (thus enhancing computational performance). Here the peak period was set to T = 13 s, such that the maximum wave length was $\lambda \sim 150$ m. The shortest waves considered corresponded to a minimum period of T = 1.5 s, with the associated minimum wave length $\lambda \sim 4$ m. The cell size was therefore set at $\Delta x \approx 0.65$ m.

A previous study undertaken by Edesess *et al.* (2017a) for linear waves found that 75 cells per wavelength in the horizontal direction and 7 cells per wave height in the vertical direction were sufficient for mesh convergence. In the present study, such a fine mesh density could not be achieved for the highest frequency waves (with shortest wave lengths), and so a minimum of 6 cells in the horizontal direction was set for the shortest wavelengths ($\approx$ 4 m) to control the computational overhead. A mesh convergence study was conducted for the autumn data set. It was found that a relatively coarse mesh with 75 cells for the modal wave length and fewer cells for shorter periods optimized computational time whilst achieving results of satisfactory accuracy. The open-source meshing tool GMSH was used to create the mesh. Grading was applied to cells at the free surface, with cells coarsened towards the top and bottom of the domain to reduce their overall number.

In order to utilise data from the offshore wind farm location, Dirichlet boundary condition values in the frequency regime were obtained from the spectrum of the field data $S_{\eta,data}$. The boundary input condition introduced here, *customSpectrum*, comprised the computed free surface elevation and horizontal and vertical water particle velocity component time series from the seasonal wave energy spectrum using (3)-(6) in conjunction with the linear dispersion equation.

A symmetry condition was applied at lateral walls and a slip wall condition was applied at the bottom of the domain. Stability was achieved through an adjustable time step, dependent on the Courant condition, whereby

$$Co = \frac{\Delta t |U|}{\Delta x} \leq 0.5, \quad (11)$$

where Δt is the time step, Δx is the cell dimension and $|U|$ is the velocity magnitude in the cell.

4. Results

Four simulations were completed, covering spring, summer, autumn and winter conditions for the open sea. All simulations were run in parallel using 24 processors on a supercomputer operated by the Irish Centre for High End Computing. For the two bi-modal sea states (winter and summer), a much greater mesh density was needed to capture properly the shortest wavelengths, which greatly increased the computational time. Details are given in Table 1 where the total CPU given is for a simulation duration of $t^* = 30$, where $t^* = {}^{t}/_{T_p}$.

Table 1. Total CPU hours for each simulation

Season	Min λ(m)	Max λ(m)	No. Elements	CPU Time
autumn	12.7	164	786,050	4 h 10 min
winter	4.3	290	1,330,550	14 h 50 min
spring	7.7	178.6	882,050	5 hr 48 min
summer	4.3	164	1,580,040	17 hr 10 min

The driving boundary condition, *customSpectrum*, was used to input verified spectral information derived from the raw field data into the OpenFOAM® simulations. Spectral information was verified through a statistical analysis of the raw data and it was found that the variance of the surface elevation σ_η^2 was equivalent to the total energy within the spectral density curve m_0 for the raw, analytically calculated and simulated results. The predicted surface elevation variance $\sigma_{\eta,OF}^2$ and total energy within the spectral curve $m_{o,OF}$, obtained from the OpenFOAM® simulations, were also compared against the corresponding values from the original data and the analytical sea state. The significant wave height H_s was determined from (2).

Using the FFT technique, spectral functions of the surface elevation ($S_{\eta,Num}$) and the horizontal and vertical water particle velocity components ($S_{U_x,Num}$ and $S_{U_z,Num}$, respectively) were calculated from the predicted time series at numerical wave gauges located approximately $0.75\lambda_p$ from the inlet (where λ_p is the wavelength corresponding to T_p). The simulated spectrum function for wave energy was then compared against its counterpart calculated directly from the field data; statistical parameters, such as the variance σ_η^2, are used to verify that the simulated sea state had the correct statistical characteristics. From S_η, the peak frequency f_p was found and the modal period T_p $(= 1/f_p)$ identified for each set of data.

Figures 2-5 present the free surface elevation η time series and associated spectra obtained from the raw data, analytical sea state, and from simulations using OpenFOAM®, at the inlet of the computational domain. Figure 6a shows comparisons between the fine mesh where 100 cells per modal wave length were used and the coarser mesh where 75 cells per wavelength was used. The coarser mesh allowed for a reduction in computational time and was deemed satisfactory for the remainder of the simulations. The y-axis scale was not maintained across all figures to allow for clearer visualisation of peak values. The subscripts in the figures represent the following: "raw" is the *in situ* data set, "an" is the data from analytical predictions and "N" refers to the numerical predictions. In Figure 2b, "N1" refers to mesh 1 and "N2" is mesh 2.

Tables 2-5 list the statistical information calculated for each seasonal free surface elevation time series and the percentage error between the simulated results and the original data. For each seasonal data set, (1) was satisfied and the analytical sea state was equivalent to the raw data.

In addition to contributing to verification of the simulated sea state, such velocity data are potentially useful for determining loadings on a vessel. Figures 6a-6d display comparisons between the analytically calculated horizontal and vertical velocity spectral functions and their simulated counterparts. The agreement between the numerically and analytically calculated horizontal and vertical velocity spectral functions (S_u and S_w, respectively) provides additional corroboration that the correct sea state has been produced.

5. Discussion and Conclusions

OpenFOAM®, Waves2Foam, and the input boundary condition *customSpectrum* were used to simulate the free surface time series for irregular uni-directional waves, based on *in situ* data from Teesside Offshore Wind Farm. Numerical and analytical predictions were compared against the raw data through statistical and spectral analyses of the free surface elevation and velocity component time series. Four data sets of length 24 hours, representative of each season of the year, measured at a frequency f = 1.28 Hz during 2015/2016, were used to calibrate the input boundary condition. Following conversion of the raw data from cm to m, a FFT was performed over a range of frequencies and the wave spectrum for each relevant value was calculated and smoothed. Total energy within the spectrum was found through integration. From (3), the amplitudes for each frequency bin were calculated, which were then used to determine the sea state at the boundary.

Finally, the analytically calculated sea state was compared statistically to the raw data using (1). The sea state and statistical

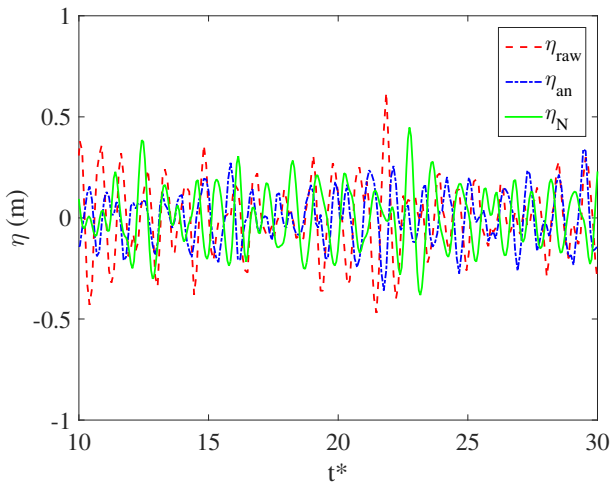

(a)Autumn free surface elevation time series

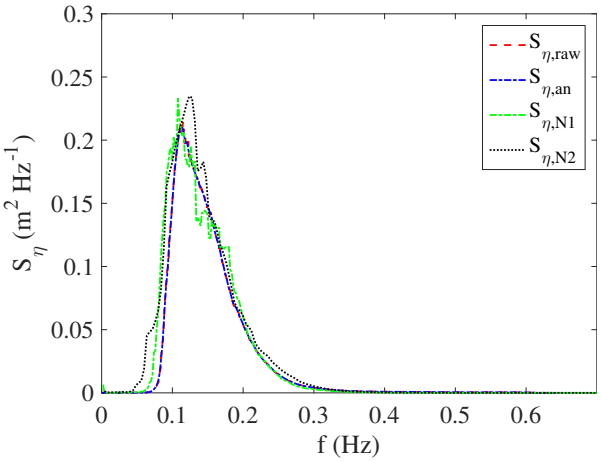

(b)Autumn wave spectrum

Figure 2. Autumn free surface time series and associated spectrum function of η

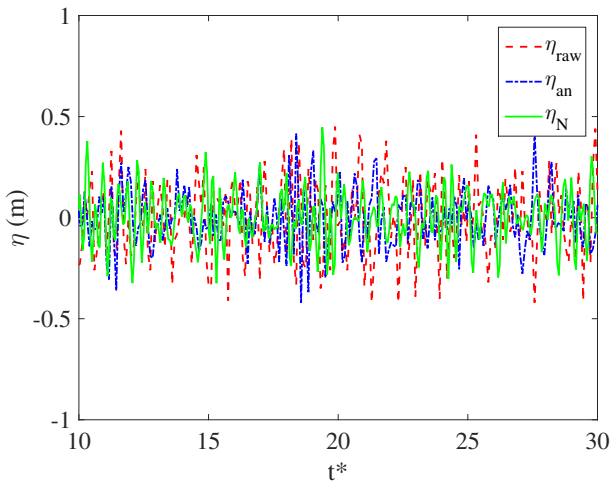

(a)Winter free surface elevation time series

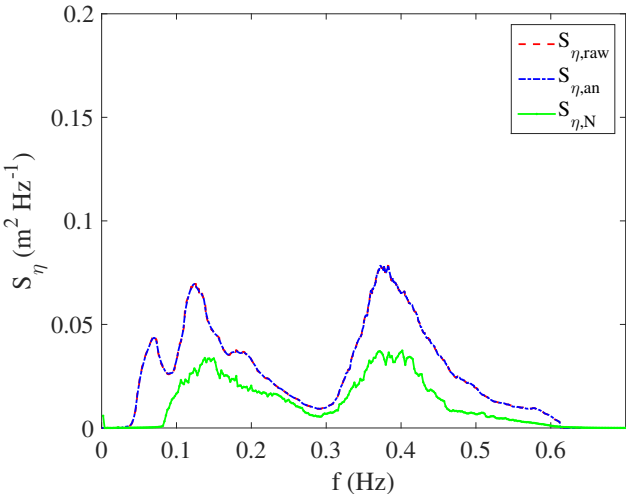

(b) Winter wave spectrum

Figure 3. Winter free surface time series and associated spectrum function of η

Table 2. Autumn Statistical Values - September 2015

	Raw data	Analytical sea state	OpenFOAM	Percentage error
$\sigma_\eta^2 = m_{0,\eta}$	0.0176 m^2	0.018 m^2	0.020 m^2	10.8 %
$H_s = \sqrt{m_0}$	0.53 m	0.53 m	0.56 m	5.1 %
T_p	8.69 s	8.69 s	8.08 s	7.1 %

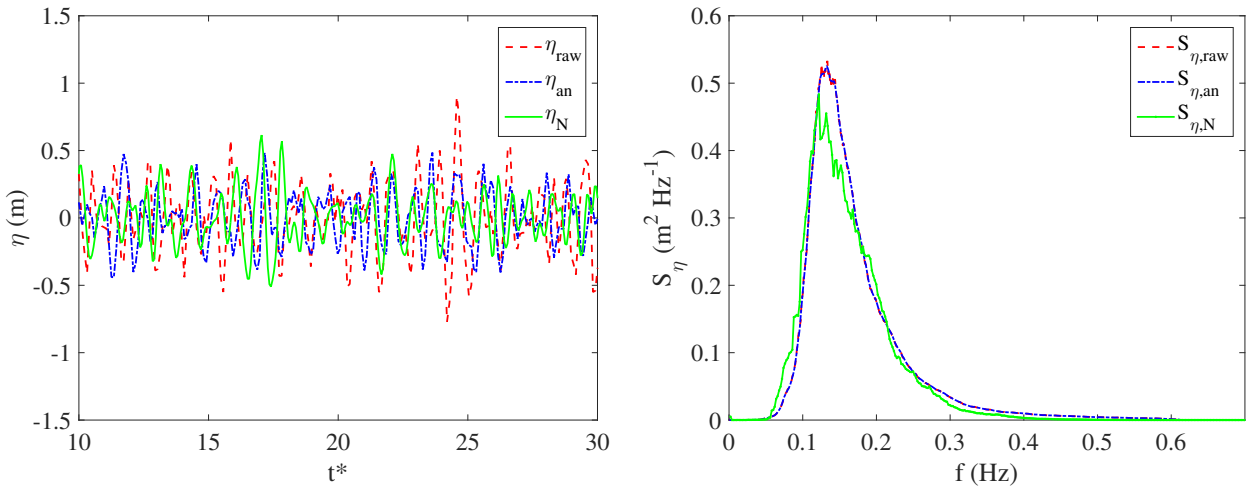

(a) Spring free surface elevation time series **(b)**Spring wave spectrum

Figure 4. Spring free surface time series and associated spectrum function of η

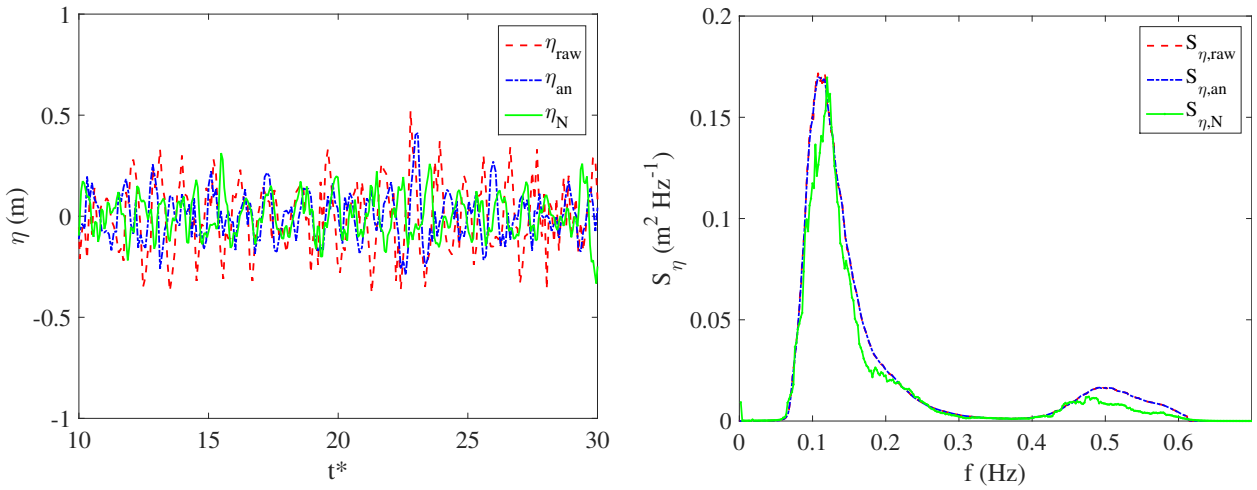

(a) Summer free surface elevation time series **(b)**Summer wave spectrum

Figure 5. Summer free surface time series and associated spectrum function of η

Table 3. Winter Statistical Values - December 2015

	Raw data	Analytical sea state	OpenFOAM	Percentage Error
$\sigma_\eta^2 = m_{0,\eta}$	0.018 m^2	0.018 m^2	0.017 m^2	5.6 %
$H_s = 4\sqrt{m_0}$	0.54 m	0.54 m	0.52 m	3.7 %
T_{p1}	8.11 s	8.11 s	7.25 s	10.6 %
T_{p2}	2.61 s	2.61 s	2.69 s	3.0 %

Table 4. Spring Statistical Values - March 2016

	Raw data	Analytical sea state	OpenFOAM	Percentage Error
$\sigma_\eta^2 = m0, \eta$	0.050 m^2	0.050 m^2	0.047 m^2	6.0 %
$H_s = 4\sqrt{m_0}$	0.89 m	0.89 m	0.87 m	2.2 %
T_p	7.50 s	7.50 s	6.80 s	9.3 %

Table 5. Summer Statistical Values - June 2016

	Raw data	Analytical sea state	OpenFOAM	Percentage Error
$\sigma_\eta^2 = m_{0,\eta}$	0.015 m^2	0.015 m^2	0.012 m^2	20.0 %
$H_s = 4\sqrt{m_0}$	0.49 m	0.49 m	0.44 m	10.2 %
T_{p1}	9.30 s	9.30 s	8.35 s	10.2 %
T_{p2}	2.03 s	2.03 s	2.09 s	3.0 %

information has been presented in Tables 2-5 for the following three datasets:

1. Raw data set composed of (η_{raw} time series and $S_{\eta,Raw}$) spectrum,
2. Analytical data set from equations (4)-(6) (η_{An}, $S_{\eta,An}$, $S_{Ux,An}$ and $S_{Uz,An}$),
3. Numerical data set from OpenFOAM® predictions of η_{OF} time series, and $S_{\eta,OF}$, $S_{Ux,OF}$ and $S_{Uz,OF}$).

It was found that, using *customSpectrum*, the simulations in OpenFOAM® were capable of capturing the significant wave height to within 10% of the raw data (with the lowest percentage difference of 3.20% for the winter significant wave height). Although the phase information was not conserved for the surface elevation time series, the results in the frequency domain exhibit good agreement between the raw data and the analytical and numerical predictions. Larger differences were found between σ_η^2 and m_0 (up to 20 % difference in the summer)

Table 1 indicates there is a significant difference in the total CPU time required to process the winter and summer datasets in comparison to the spring and autumn. This is because bi-modal spectra were generated from the December 2015 and June 2016 data, where shorter frequency waves contribute significantly to the total energy. Although the same minimum wavelength (maximum wave frequency) was used for both summer and winter data, an increase in energy at the lowest frequencies in the winter spectrum meant that longer wavelengths were included. Only 5 cells per wavelength were used for the shortest wavelengths that correspond to the second peak (the aim being to achieve accurate results while maintaining computational efficiency).

During 2015/2016 (the twelve-month period when data were gathered), the spectral density function switched between single distributions in autumn and spring to bi-modal distributions in winter and summer. There is a primary peak evident at $f \approx 0.15$ Hz related to waves aligned with the predominant wind direction. The presence of a second peak in winter and summer, which appears around $f \approx 0.4$ Hz, indicates that higher frequency waves were interacting with the local wind-wave system, decreasing energy in the first peak while increasing the energy at a higher frequency. Guedes Soares (1984) estimates that bi-modal spectra occur 5-40% of the time in the North Sea. The bi-modal spectra in Figure 3, and to a lesser degree in Figure 5, suggest that swell waves may be propagating from a distant storm at a different direction, frequency, period and wave height, merged with the locally generated wave field, altering the spectral parameters in the region (Toffoli *et al.*, 2010; Sabatino *et al.*, 2016). In the current work, the wave information has been collected by a single buoy; it has not been possible to separate the locally generated waves from swell, which may be particularly important regarding the bi-modal spectrum. Further data from several spatially separated

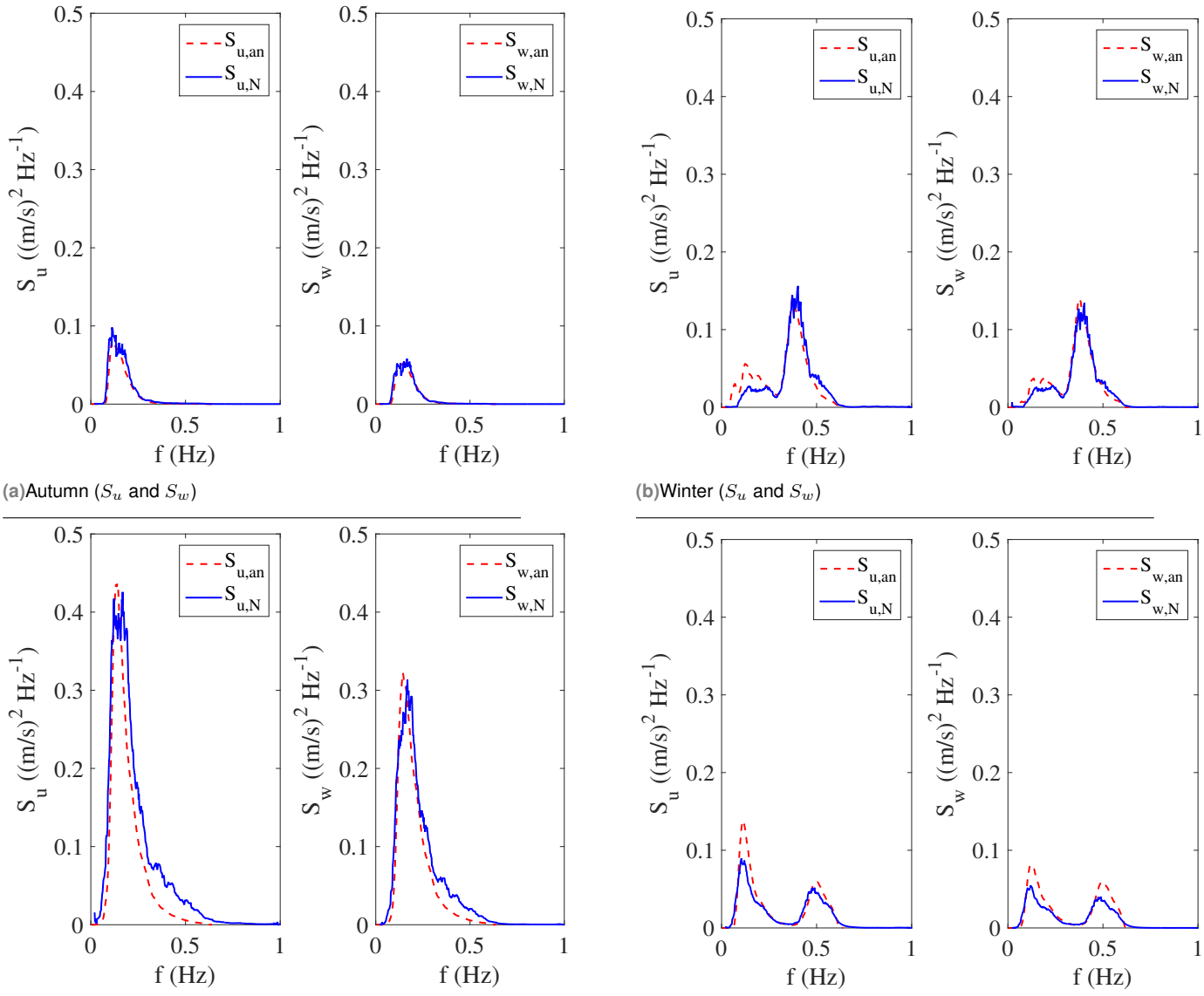

(a)Autumn (S_u and S_w)

(b)Winter (S_u and S_w)

(c)Spring (S_u and S_u)

(d)Summer (S_u and S_u)

Figure 6. Velocity spectra

buoys would be desirable to identify directionally spread and locally generated waves and their subsequent effect on the wave kinematics.

The close proximity to the shore (1.5 km) and shallowness of the offshore wind farm site (15 m) could exacerbate such spectral changes, when external storm swells interact with the local sea state. Historical statistical weather data in the southern North Sea, near the Teesside offshore wind farm site, show a wind direction predominantly in the southwest direction in March and September, whilst the June data exhibit a larger spread in the northeast direction and the December data exhibit a more southerly dominated wind direction [†], the direction change accounting for the second peak appearing in the spectrum.

[†] see https://www.windfinder.com/windstatistics/Teesside

The present analysis assumes that the sea state is uni-directional. However, the historical weather data indicate the sea state is more likely to be multi-directional with crossing seas. A better representation would therefore be to use two directional spreading functions, one for each modality, to improve the accuracy of the computational model. However, data for this work was only available for a single wave buoy at one location, greatly limiting the degree to which directionality can be determined (McAllister *et al.*, 2017). Whilst inclusion of directionality is beyond the scope of the present paper, a multi-directional model that can resolve the prevailing wind-wave-swell directions from single point wave observations (see e.g. Adcock & Taylor (2009)) could be developed to improve the model.

The results presented confirm that the combination of *customSpectrum* and OpenFOAM® provided a useful preliminary method for engineers to simulate the free surface wave motions present at the site of an offshore wind farm. The main contribution of the paper is that it demonstrates that observed data from a wave buoy at an offshore wind farm site can be used to generate useful input conditions to a simulation model. The second paper in this set applies the input conditions calibrated here to a simulation describing the interaction with the turbine monopile support column. Engineers can benefit greatly by computing accurate site-specific wave conditions, rather than relying on a parametric representation of the wave conditions. By determining the ocean wave spectrum from wave buoy observations and then simulating random sea states, the *custom Spectrum* boundary condition has been calibrated for use in numerical simulations of wave conditions at Teesside Offshore Wind Farm, for four different seasons throughout a year. The approach accounts for seasonal changes between uni-modal and bi-modal spectra that occurred in the year of interest.

The model is designed for uni-directional seas, and is also capable of providing an estimate of the lower-frequency peak in a bi-modal spectrum, although the accuracy of the model will be greatly diminished for multi-directional or crossing seas. In addition, the values presented here are the results from only a single year of data; improvements could be made from a longer data sample, taking into account climate affects that can occur over years rather than months. In order to investigate the hypothetical limitations of the model, it would be worth undertaking simulations of multi-directional spread seas and perhaps crossing seas and comparing the model results to the hypothetical sea states.

Improved accuracy of significant wave height values at an offshore wind farm is important to CTV operators who rely on such information to determine the feasibility of accessing the turbines for repair. Assembling a database of simulated sea states based on additional data collected at the offshore wind farm site would improve the calibration of *customSpectrum* and thus provide a more realistic simulation of the sea state incident on CTVs for a wider range of sea states. To advance this work, *customSpectrum* could be applied as an input boundary condition to simulate waves numerically in a specified sea state interacting with a surface-piercing monopile. CTV motion could then be computed using a standard 2D vessel-motion method, such as strip theory, where it is assumed that the vessel displacement varies linearly with the diffracted wave velocities and accelerations (Journee & Pinkster, 2002).

Acknowledgements

This research was made possible thanks to the *in situ* data contribution from the Operations Team at EDF Energy Renewables Teesside Offshore Wind Farm. We are also grateful to Dr. Tariq Dawood for his assistance with information on the Teesside wind farm site. This research was supported by MaREI - Marine and Renewable Energy Ireland and also partially funded by Alexis Billet of Resilience Energy Ltd., without whose knowledge and support this research could not be completed.

REFERENCES

Adcock TAA & Taylor PH (2009) Estimating ocean wave directional spreading from an eulerian surface elevation time history. *Proceedings of the Royal Society A* **465**: 3361–3381, 10.1098/rspa.2009.0031.

Auckland R & Garlick R (2015) *Wind Farm Service Vessels (WFSVs) - An Analysis of Supply and Demand. Technical Report 44*, 4COffshore.

Baagøe-Engels V & Stentoft J (2016) Operations and maintenance issues in the offshore wind energy section: An explorative study. *International Journal of Energy Sector Management* **10(2)**: 245–265.

Breton SP & Moe G (2009) Status, plans and technologies for offshore wind turbines in europe and north america. *Renewable Energy* **34(3)**: 646–654.

Browell J, Dinwoodie I & McMillan D (2016) Forecasting for day-ahead offshore maintenance scheduling under uncertainty. In *European Safety and Reliability Conference*, The University of Strathclyde, Glasgow.

Capps S & Zender C (2010) Estimated global ocean wind power potential from quikscat observations, accounting for turbine characteristics and siting. *Journal of Geophysical Research* **115**: 13, 10.1029/2009JD012679.

Corbetta G, Pineda I & Moccia J (2014) *The European offshore wind industry - key trends and statistics 2013*. *Technical report*, European Wind Energy Association.

Dalgic Y, Lazakis I & Turan O (2015a) Investigation of optimum crew transfer vessel fleet for offshore wind farm maintenance operations. *Wind Engineering* **39(1)**: 31–52.

Dalgic Y, Lazkis I, Dinwoodie I, McMillan D & Revie M (2015b) Advanced logistics planning for offshore wind farm operation and maintenance activities. *Ocean Engineering* **101**: 211–226.

Dean RG & Dalrymple RA (1991) *Water Wave Mechanics for Engineers and Scientists*. World Scientific Publishing Co. Pte. Ltd., London.

Edesess AJ, Kelliher D, Borthwick AGL & Thomas G (2017a) Preliminary analysis of free surface flow around a surface-piercing cylinder using openfoam in the context of maintenance operations related to offshore wind farms, accepted for publication in the 11th OpenFOAM Workshop Book.

Edesess AJ, Kelliher D, Borthwick AGL & Thomas GP (2017b) Improving global accessibility to offshore wind power through decreased operations and maintenance costs: a hydrodynamic analysis, accepted for publication in Energy Procedia.

Guedes Soares C (1984) Representation of double-peaked sea wave spectra. *Ocean Engineering* **11**: 185–207.

Halvorsen-Weare EE, Gundegjerde C, Halvorsen IB, Hvattum LM & Nonås LM (2013) Vessel fleet analysis for maintenance operations at offshore wind farms. *Energy Procedia* **35**: 167–176.

Hoffman M (2011) A review of decision support models for offshore wind farms with an emphasis on operation and maintenance strategies. *Wind Energy* **35(1)**: 1–16.

Jacobsen NG, Fuhrman DR & Fredsoe J (2011) A wave generation toolbox for the open-source cfd library: Openfoam. *International Journal for Numerical Methods in Fluids* **70**: 1073–1088.

Josse T, Billet A & Leen SB (2011) Prediction of supply vessel motion during transfer to a fixed structure. In *Proceedings of the 30th International Conference on Ocean, Offshore and Arctic Engineering*.

Journee JMJ & Pinkster J (2002) *Introduction to Ship Hydrodynamics*. Delft University of Technology.

Kieffer G & Couture TD (2015) *Renewable Energy Target Setting*. *Technical report*, International Renewable Energy Agency (IRENA).

König M, Gonzlez DF, Abdel-Maksoud M & Düster A (2017) Numerical investigation of the landing manoeuvre of a crew transfer vessel to an offshore wind turbine. *Ships and Offshore Structures* **12**: S115–S133, 10.1080/17445302.2016.1265883.

Krewitt W, Nienhaus K, Klessmann C, Capone C, Stricker E & Graus W (2009) *Role and potential of renewable energy and energy efficiency for global energy supply*. *Technical Report (UBA-FB) 001323/E*, Dessau-Rosslau: Federal Environment Agency (Umweltbundesamt).

Le Mehaute B (1976) *An Introduction to Hydrodynamics and Water Waters*. Springer.

Maples B, Saur G, Hand M, van der Pieterman R & Obdam T (2013) *Installation, Operation, and Maintenance Strategies to Reduce the Cost of Offshore Wind Energy*. *Technical report*, National Renewable Energy Laboratory (NREL), Golden, CO.

McAllister ML, Venugopal V & Borthwick AGL (2017) Wave directional spreading from point field measurements. *Proceedings of the Royal Society A* **473**: 20160781.

Papoulis A (1991) *Probability, Random Variables, and Stochastic Processes*. 3rd edn., McGraw-Hill, Inc., United States.

Pineda I (2016) *The European offshore wind industry - key trends and statistics 2015*. *Technical report*, European Wind Energy Association (EWEA).

Sabatino AD, McCaig C & Heath RBOMMR (2016) Modelling wave-current interactions off the east coast of scotland. *Ocean Science* **12**: 875–897.

Sperstad IB, Halvorsen-Weare EE, Hoffman M, Nonas LM, Stalhane M & Wu M (2014) A comparison of single- and multi-parameter

wave criteria for accessing wind turbines in strategic maintenance and logistics models for offshore wind farms. In *EERA DeepWind' 2014, 11th Deep Sea Offshore Wind R&D Conference*, vol. 53, pp. 221–230.

Sumer BM & Fredsøe J (2006) *Advanced Series on Ocean Engineering - Hydrodynamics Around Cylindrical Structures*, vol. 26. World Scientific Publishing Co. Pte. Ltd., Singapore.

Toffoli A, Onorato M, Bitner-Gregersen EM & Monbaliu J (2010) Development of a bimodal structure in ocean wave spectra. *Journal of Geophysical Research* **115(C3)**: C03006.

van Bussel GJW, Henderson AR, Morgen CA, Smith B, Barthelmie R & Argyriadis K (2001) State of the art and technology trends for offshore wind energy: Operation and maintenance issues. In *Proceedings of Offshore Wind Energy Special Topic Conference*, Brussels, Belgium.

List of Figures

List of Tables